Biomimetic Composites

DOI: 10.1002/anie.200800968

Shape Development and Structure of a Complex (Otoconia-Like?) Calcite–Gelatine Composite**

*Ya-Xi Huang, Jana Buder, Raul Cardoso-Gil, Yurii Prots, Wilder Carrillo-Cabrera, Paul Simon, and Rüdiger Kniep**

A large number of recent publications deal with control of the size and shape of calcium carbonate in its calcite modification by organic additives acting as growth modifiers or templates.[1–8] Other reports focus not only on shape control but also on the control of the calcium carbonate modification formed.[9–14] Only a few publications concentrate on calcite specimens showing a habit that is more or less close to the shape of biogenic (calcite) otoconia (see Figure 1), characterized by their barrel-shaped habit with triplanar faceted ends. These include spindle-shaped, rhombohedrally truncated specimens obtained in the presence of malonic acid,[15] the development of additional (sometimes even structured) faces extending nearly parallel to the *c*-axis direction in the presence of γ-carboxyglutamate or α-aminosuccinate,[16] malic acid together with urea,[17] glycoproteins extracted from sea-urchin spines,[18] and nacre proteins.[19]

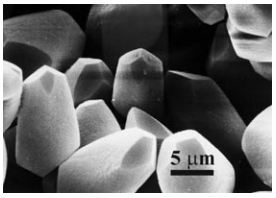

Figure 1. Scanning electron microscopy (SEM) image of calcite otoconia of guinea pig showing a barrel-shaped habit with triplanar faceted ends.[26–28] Otoconia ("ear-dust") are part of the so-called maculae inside the inner ear of mammals, which act as gravity receptor organs responding to linear accelerations.[37]

It is not clear at present whether the organic components under consideration and acting as growth modifiers are generally incorporated into the solid to form an inorganic–organic composite material, but some indications have already been reported with respect to incorporation of the organic component into the calcite host (sea-urchin proteins[20] as well as gelatine[21]). More recent investigations deal with the incorporation of agarose gel fibers into porous calcite single crystals and the resulting (moderate) changes in morphology.[22,23] Changes in the morphology of calcite crystals are also observed in the presence of inorganic additives, such as Mg^{2+} ions. With increasing amounts of Mg^{2+} (added as $MgCl_2$ to the solutions), the calcite crystals show a more pronounced development of (101) faces which combine with the typical rhombohedral faces.[24] In a more detailed investigation[25] it was shown that incorporation of Mg^{2+} into a growing calcite crystal causes strain at the intersection of compositionally distinct growth steps, thus leading to the emergence of pseudofacets, which finally results in apparent elongation of the crystal. This kind of shape elongation along [001] is similar to that produced by some organic additives as discussed above.[15–19]

In the present work, complex calcite–gelatine composite particles were grown by double diffusion in gelatine gel matrices (see the Experimental Section). The composite specimens grow close to the calcium-ion source; the development of their complex shape is shown in Figure 2. Within five days the morphogenesis leads from shape 1 (an arrangement characterized by six trumpetlike branches) to various intermediate states that are still dominated by six branches (shapes 2–7). The branches grow fast and develop their basal faces to the final state (shape 8) where they meet at both ends, thereby forming three planar faces with straight common edges and rounded boundaries in the direction of the belly region. This region grows with temporal delay and appears to be structured on a small particle scale but with a preferred (common) orientation of subunits.

Apart from the more pronounced and rounded belly region, the calcite–gelatine composite specimens in their final state of development show morphological characteristics similar to those for adult otoconia of mammals, with an overall symmetry close to $\bar{3}m$ (see Figure 1). As concerns their size, the artificial specimens have to be classified as "more than giant" (the mean length of biogenic otoconia is about 10 μm,[29] but "giant" otoconia up to 80 μm in length are also observed).[30] Samples investigated after a growth period of five days consist of composite particles in their final state of shape development with a size distribution between 100 μm and 400 μm. Initial observations indicate that development of

[*] Dr. Y.-X. Huang, J. Buder, Dr. R. Cardoso-Gil, Dr. Yu. Prots, Dr. W. Carrillo-Cabrera, Dr. P. Simon, Prof. Dr. R. Kniep
Max-Planck-Institut für Chemische Physik fester Stoffe
Nöthnitzer Straße 40, 01187 Dresden (Germany)
Fax: (+49) 351-4646-3002
E-mail: kniep@cpfs.mpg.de

[**] We gratefully acknowledge the Fonds der Chemischen Industrie for generous support. We are also grateful to Dr. G. Auffermann and A. Völzke for elemental analyses, H. Dallmann (TU Dresden) for thermal analyses, and Dr. U. Burkhardt for density measurements. We thank Prof. H. Lichte (TU Dresden) for the possibility to perform TEM measurements at the Triebenberg Laboratory and Dr. S. Wirth for fruitful discussions. Finally, we thank Prof. T. Zahnert and Dr. Y. Yarin (Universitätsklinikum der TU Dresden) for the SEM images of biogenic otoconia; coloring of the images was performed by Dipl.-Ing. H. Tlatlik (MPI CPfS).

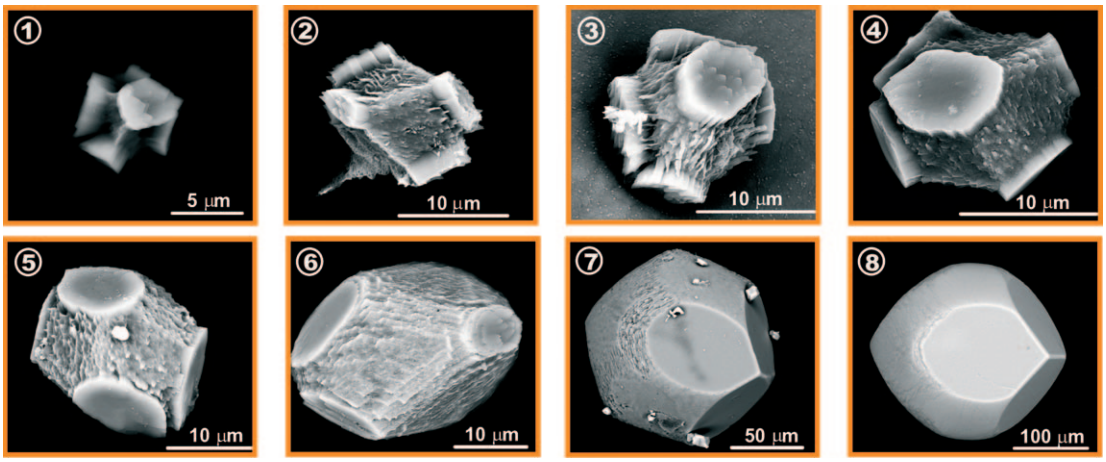

Figure 2. Shape development (sequence 1–8) of the calcite–gelatine composite. Development starts with an arrangement of six rhombohedral branches. The growing branches take control of the morphogenesis and the belly region is filled with small but oriented calcite particles by temporal delay. The morphogenesis is finished after about five days when the conelike, rhombohedral branches meet at both ends of the individual specimen, thereby forming three planar faces with straight common edges and a rounded "fence" in the direction of the belly region.

the shape to the "closed otoconial habit" may, in general, finish at a composite size of around 100 μm. This assumption, however, needs further investigation.

As summarized in Figure 3, the calcite–gelatine composite exhibits scattering properties representative of a single crystal, and even the crystal structure (calcite) could be solved by using a complete single specimen. These scattering properties that are closely related to those of a single crystal are particularly remarkable when taking into account the shape development shown in Figure 2, and indicate the formation of a mosaic-controlled nanocomposite superstructure similar to that reported for biomimetic apatite–gelatine nanocomposites.[31–35] This kind of solid matter is also called a "mesocrystalline" state.[36] In fact, the as-grown individual particles represent an inorganic–organic composite containing an amount of gelatine between 1.9 (Figure 3; thermogravimetric analysis (TGA)) and 2.6 wt % (chemical analysis; see the Experimental Section). The composite nature of the individuals is associated with a lower density (2.563 $g\,cm^{-3}$) compared with that of a bulk calcite crystal (2.711 $g\,cm^{-3}$). As can also be seen from Figure 3, the planar terminal faces are indexed as "normal" rhombohedral faces (cleavage rhombohedra of calcite), and initial investigation of the inner architecture of the individuals by SEM shows the presence of two different structures: a more dense homogeneous and a more porous structure.

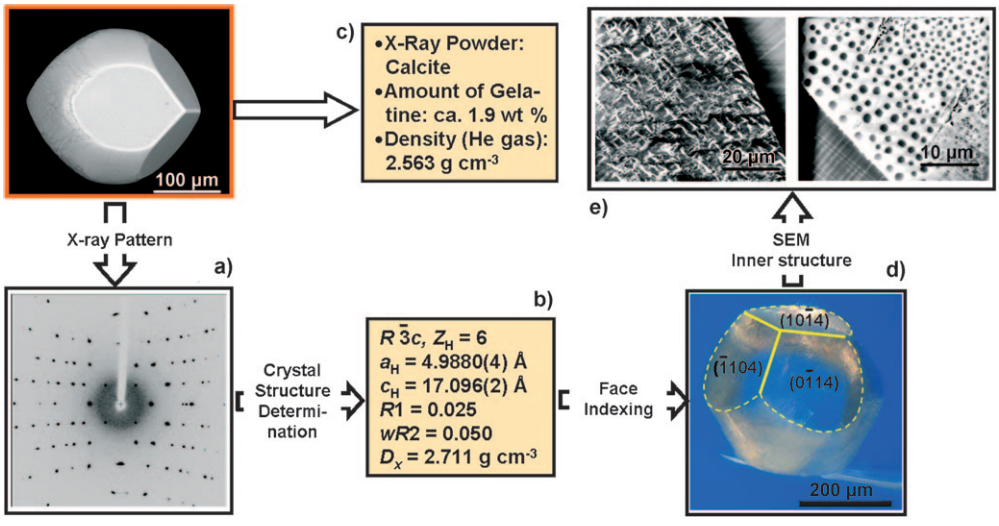

Figure 3. Characterization of a completely developed calcite–gelatine composite specimen (top left; see the Experimental Section for details). a) The composite specimen exhibits X-ray scattering properties which are representative of a single crystal. b) The crystal structure of calcite was solved from single-crystal diffraction data. c) The density of the composite (He gas method) is significantly lower than that of a calcite crystal; 1.9 wt% of gelatine contributes to the formation of the composite. d) The faces at both ends of the otoconia-shaped specimen were determined as "normal" rhombohedral faces (=cleavage rhombohedra of calcite). e) SEM images of the inner architecture of the biomimetic composite indicate a porous structure in the belly region and a more dense structure in the branch areas.

This first SEM observation (Figure 3) was followed by a more detailed TEM investigation by means of a thin focused-ion-beam (FIB) cut through the branch and belly regions of a calcite–gelatine composite specimen in an early growth state (Figure 4). It became clear that the branch area is characterized by a dense composite structure streaked with parallel traces about 10 nm in thickness. In analogy to our experience with apatite–gelatine nanocomposite structures[31–35] and in accordance with the hollow tubes visible in par-

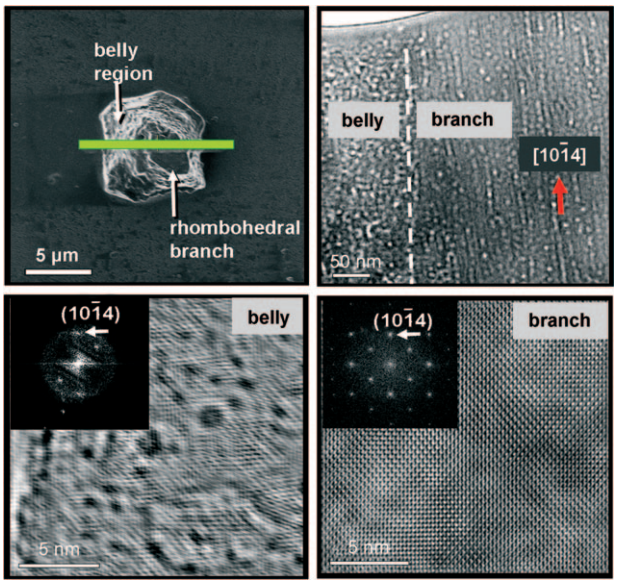

Figure 4. Top left: Ion-scanning image of a calcite–gelatine composite individual at an early stage of morphogenesis (see Figure 2). The green bar indicates the area from which the TEM lamella was cut by the FIB technique. The cut leads through one branch oriented along the view direction. Top right: Overview TEM image of the FIB thin cut showing the structure of the composite consisting of two different areas (belly and branch), which are clearly distinguished by their different patterns of bright spots (produced by voids and/or the organic component of the composite). The branch part (right) reveals parallel traces about 10 nm in thickness corresponding to calcified microfibrils stretching out along the main branch direction [10$\bar{1}$4]. The belly part (left) shows a less-ordered structure consistent with the observations (Figure 2) made during shape development. Bottom right: The filtered high-resolution TEM image reveals that the branch shows a perfect periodic pattern. Deduced from the fast Fourier transform (FFT; inset), the calcite composite is viewed along [42$\bar{6}\bar{1}$]. Bottom left: The belly region is only poorly crystalline and consists of nanodomains in a mosaic arrangement and of pores. Compared with the branch area, the FFT of the belly region (inset) shows only a small number of weak spots as a result of reduced crystallinity. However, the overall crystallographic orientation of the belly and branch areas of the biomimetic specimen is identical and leads to X-ray scattering properties of the individuals that are representative of a single crystal (see Figure 3 and the Experimental Section).

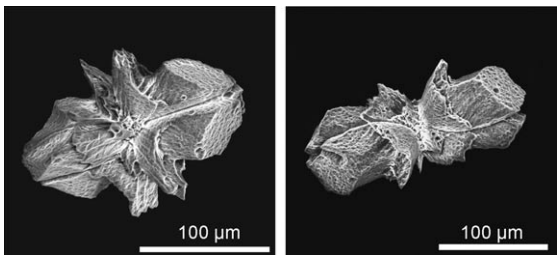

Figure 5. SEM images of calcite–gelatine composite individuals after partial decalcification by EDTA followed by treatment with water to remove residual amounts of gelatine from the surface. For further details, see text.

tially decalcified composite individuals (Figure 5), we interpret these traces as corresponding to calcified microfibrils stretching out along the main branch direction [10$\bar{1}$4]. The high-resolution TEM image of the branch area shows a perfect periodic calcite pattern. The belly region, on the other hand, is only poorly crystalline and consists of nanodomains in a mosaic arrangement and of pores. The overall crystallographic orientation of the belly and branch areas is identical (see FFTs in Figure 4), an observation that fully agrees with the scattering properties of the biomimetic otoconia (similar to that of a single crystal).

As shown in Figure 5, the calcite–gelatine composite individuals can be decalcified by treatment with ethylenediaminetetraacetate (EDTA; the gelatinous residue thereby keeps the shape of the former composite). Such a type of (partial) decalcification helps to give a deeper insight into the inner architecture of the artificial specimens as well as into the structural correlations between the inorganic and organic components. These investigations may also give the chance to find and isolate the central seed area that keeps the intrinsic code for this particular kind of shape development. The SEM images (Figure 5) were taken after partial decalcification followed by treatment with water to remove residual amounts of gelatine from the surface. In accordance with the TEM investigations that indicate a more dense structure for the branches (Figure 4), the SEM images (Figure 5) clearly show that these regions are less soluble compared with the porous and less-ordered belly area. It is also evident from the SEM images that the interactions between the organic and inorganic components of the composite take place at a high level of structural order. The hollow tubes appearing on the rhombohedral faces represent the positions of the former organic fibrils extending from the center of the architecture in the direction of the faces at both ends of the specimen (see also Figure 4).

Relationships between the artificial calcite–gelatine composite and biogenic otoconia have already been pointed out in relation to the outer shape and symmetry of the individual particles. But even the inner architectures of the biogenic and artificial composite specimens are closely related: at least two different kinds of structure are present in biogenic otoconia, a more dense one and a more porous one.[28] It was also reported that a higher material density seems to be present in the direction towards the rhombohedral end-faces.[38] Further observations revealed that (at least parts of) the biogenic otoconial specimen behave like single crystals.[39–41] The shape development of the artificial composite individuals (Figure 2) and their decalcification behavior (Figure 5) clearly show that there are three distinct growth directions for the branch areas which are orientated to the planar faces of the specimens (rhombohedral symmetry). The branch areas meet at the end of shape development but do not grow perfectly into a single one: there is still a significant boundary plane between the branch parts.

In a very early SEM investigation, Hommerich and Kniep observed three different regions in the fracture area close to the triplanar faceted ends of biogenic otoconia from guinea pig.[42] Figure 6 shows a more recent SEM image of the fracture area close to the triplanar faceted ends of otoconia from guinea pig, clearly revealing the presence of three distinct regions. Bearing in mind the complex inner architec-

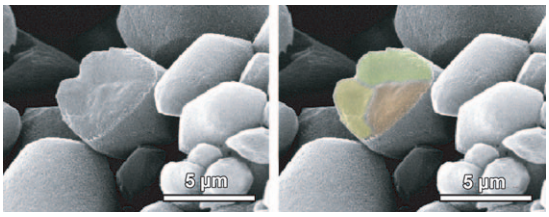

Figure 6. Left: SEM image of guinea pig otoconia. Right: the same image with colored fracture area. For further details, see text. (Image taken by Y. Yarin, Dresden University of Technology.)

ture of such individual specimens, it is evident that a deeper insight into their 3D structure can only be reached through well-defined directions (with respect to the outer shape) in which the investigations are performed. To the best of our knowledge, no complete picture of the 3D structure and no definite data on the chemical composition of biogenic otoconia are available. The same is true for the morphogenesis of biogenic otoconia. We therefore consider the shape development of the artificial composite as a suitable growth model for the biogenic individual structures.

A final point is dedicated to the nature of the organic components in both the biogenic and artificial composite specimens. Otoconia of mammals are reported to contain glycoproteins and glycosaminoglycans that form fibrils inside the composite structure.[28,39,43] Glycoproteins and glycosaminoglycans consist of macromolecules containing covalent interconnections between proteins and oligo- and polysaccharides, respectively. The artificial otoconia-shaped composite, however, is grown in a pure gelatine gel matrix. Following this knowledge on the organic components in biogenic otoconia, we simply mixed agar with gelatine and used the gel mixture as the diffusion matrix.[44] Interestingly, the more bulbous belly region can be flattened and elongated, and clearly reveals a closer relationship to the shape of otoconia of mammals as shown in Figure 7 compared with the shape of than human otoconia.[38] The characterization of the outer shape of otoconia (artificial as well as biogenic) is still on a descriptive level, as no definite rules are known concerning aspect ratios and other quantifying criteria. This is an interesting problem to be solved in the near future but, first of all, a detailed knowledge of the basic growth principles on all relevant length scales is needed.

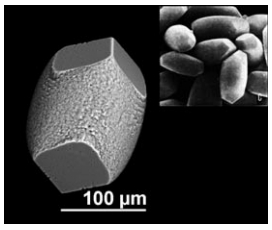

Figure 7. Artificial calcite composite individual grown in a mixed agar–gelatine gel matrix[44] compared with the shape of human otoconia (inset).[38] For further details, see text.

Experimental Section

The growth of calcite–gelatine composites was carried out in U-tubes according to the double-diffusion technique at 25 °C. The horizontal tube (10 mm in diameter, 30 mm in length) of the diffusion cell was filled with a pig-skin gelatine gel (300 bloom, Aldrich; gelatine concentration: 10 wt %). Two L-shaped tubes filled with aqueous ionic solutions, and adjusted to the physiological pH of 7.40 by addition of tris(hydroxymethyl)methylamine/HCl, were then attached to the central tube of gel. The ion concentrations in the L-shaped tubes were 1) 0.133 mol L^{-1} $CaCl_2$ and 2) 0.399 mol L^{-1} Na_2CO_3 (up to 0.027 mol L^{-1} NaF can be added as mineralizing agent). The formation of otoconia-shaped calcite–gelatine composites was observed close to the calcium source. The double-diffusion experiments were run for periods between 5 and 10 days. The gelatine plug was then pressed out of the central tube and cut into slices corresponding to the Liesegang bands formed. To isolate the solid aggregates the slices were washed several times with hot water and centrifuged.

X-ray powder diffraction experiments were carried out on a Huber image plate Guinier camera G 670; the calcite–gelatine composite specimens in different growth states were identified as calcite. Single-crystal X-ray diffraction of a calcite–gelatine composite individual in its final morphogenetic state was performed on a Rigaku AFC 7 four-circle diffractometer equipped with a Mercury CCD detector ($Mo_{K\alpha}$ radiation, graphite monochromator, scanning types: ϕ and ω) at 22 °C. The crystal structure was solved and refined in the space group $R\bar{3}c$ ($a = 498.80(4)$, $c = 1709.6(2)$ pm, $Z = 6$, $V = 368.36(6) \times 10^6$ pm^3; Ca: 0, 0, 0; O: 0.5903(3), 2/3, 11/12; C: 1/3, 2/3, 11/12; $R1 = 0.025$, $\omega R2 = 0.050$).

TGA of the calcite–gelatine composites was performed on a Netzsch STA 409 apparatus. The weight loss of 1.9 % occurring between 200 and 600 °C was assigned to the loss of gelatine (after drying between room temperature and 150 °C). CO_2 (42.3 wt %) from $CaCO_3$ was released between 650 and 850 °C; this curve exactly follows that of pure calcite.

Chemical analyses were performed with a Vista inductively coupled plasma–optical emission spectrometer (Varian) for Ca and a Leco CHNS-932 analyzer for C and N. The lower content of Ca (obs.: 38.5(1)/calc.: 40.04 wt % for pure calcite) and the higher content of total carbon (obs.: 12.46(5)/calc.: 12.00 wt % for pure calcite) are consistent with the additional presence of the organic component (gelatine). The N content within the composite (obs.: 0.43(1) wt %) represents the amount of gelatine and results in about 2.6 wt % gelatine for the composite by taking into account the fact that pure gelatine contains 16.5(1) wt % N (experimental data). Compared with an amount of 1.9 wt % gelatine (from TG measurements, see above), the value of 2.6 wt % is of a similar order and thus acceptable with respect to all errors that can be made in bulk analyses of this complex composite system.

Face indexing of an otoconia-shaped specimen in its final state of development was performed by using the X-shape 1.03 Crystal Optimization for Numerical Absorption Correction procedure (Stoe & Cie GmbH). SEM images were obtained with a FEI Quantum 200 field-emission gun (FEG) system. For microstructural investigations, particles were embedded in epoxy resin (Struers Epofix) and cut with an ultramicrotome. In attempt to study the inner architecture of the biomimetic otoconia in more detail, the FIB technique (FEI Quanta 200 3 D) was used to produce thin lamellae. TEM investigations were carried out with a Philips CM 200 FEG.

Received: February 28, 2008
Revised: July 14, 2008
Published online: September 22, 2008

Keywords: biomimetic synthesis · calcite · crystal growth · nanostructures · organic–inorganic hybrid composites

[1] H. Cölfen, *Macromol. Rapid Commun.* **2001**, *22*, 219 – 252.
[2] D. Braga, *Angew. Chem.* **2003**, *115*, 5702 – 5704; *Angew. Chem. Int. Ed.* **2003**, *42*, 5544 – 5546.
[3] A. Sugawara, T. Ishii, T. Kato, *Angew. Chem.* **2003**, *115*, 5457 – 5461; *Angew. Chem. Int. Ed.* **2003**, *42*, 5299 – 5303.
[4] S. Tugulu, M. Harms, M. Fricke, D. Volkmer, H.-A. Klok, *Angew. Chem.* **2006**, *118*, 7619 – 7623; *Angew. Chem. Int. Ed.* **2006**, *45*, 7458 – 7461.
[5] S. Burazerovic, J. Gradinaru, J. Pierron, T. R. Ward, *Angew. Chem.* **2007**, *119*, 5606 – 5610; *Angew. Chem. Int. Ed.* **2007**, *46*, 5510 – 5514.
[6] B. Wucher, W. Yue, A. N. Kulak, F. C. Meldrum, *Chem. Mater.* **2007**, *19*, 1111 – 1119.
[7] A. N. Kulak, P. Iddon, Y. Li, S. P. Armes, H. Cölfen, O. Paris, R. M. Wilson, F. C. Meldrum, *J. Am. Chem. Soc.* **2007**, *129*, 3729 – 3736.
[8] O. Grassmann, R. B. Neder, A. Putnis, P. Löbmann, *Am. Mineral.* **2003**, *88*, 647 – 652.
[9] L. Addadi, S. Weiner, *Angew. Chem.* **1992**, *104*, 159 – 176; *Angew. Chem. Int. Ed. Engl.* **1992**, *31*, 153 – 169.
[10] G. Falini, S. Albeck, S. Weiner, L. Addadi, *Science* **1996**, *271*, 67 – 69.
[11] G. Falini, S. Fermani, M. Gazzano, A. Ripamonti, *Chem. Eur. J.* **1997**, *3*, 1807 – 1814.
[12] J. Zhan, H.-P. Lin, C.-Y. Mou, *Adv. Mater.* **2003**, *15*, 621 – 623.
[13] S. Thachepan, M. Li, S. A. Davis, S. Mann, *Chem. Mater.* **2006**, *18*, 3557 – 3561.
[14] Q. Meng, D. Chen, L. Yue, J. Fang, H. Zhao, L. Wang, *Macromol. Chem. Phys.* **2007**, *208*, 474 – 484.
[15] *Biomineralization: Chemical and Biochemical Perspectives* (Eds.: S. Mann, J. Webb, R. J. P. Williams), VCH, Weinheim, **1989**.
[16] *Biomineralization: Principles and Concepts in Bioinorganic Materials Chemistry* (Ed.: S. Mann), Oxford University Press, Oxford, **2001**.
[17] Z. Mao, J. Huang, *J. Solid State Chem.* **2007**, *180*, 453 – 460.
[18] S. Albeck, S. Weiner, L. Addadi, *Chem. Eur. J.* **1996**, *2*, 278 – 284.
[19] G. Fu, S. R. Qiu, C. A. Orme, D. E. Morse, J. J. De Yoreo, *Adv. Mater.* **2005**, *17*, 2678 – 2683.
[20] A. Berman, L. Addadi, S. Weiner, *Nature* **1988**, *331*, 546 – 548.
[21] O. Grassmann, G. Müller, P. Löbmann, *Chem. Mater.* **2002**, *14*, 4530 – 4535.
[22] H. Li, L. A. Estroff, *J. Am. Chem. Soc.* **2007**, *129*, 5480 – 5483.
[23] H. Li, L. A. Estroff, *CrystEngComm* **2007**, *9*, 1153 – 1155.
[24] D. Kralj, J. Kontrec, L. Brecevic, G. Fallini, V. Nöthig-Laslo, *Chem. Eur. J.* **2004**, *10*, 1647 – 1656.
[25] K. J. Davis, P. M. Dove, L. E. Wasylenki, J. J. De Yoreo, *Am. Mineral.* **2004**, *89*, 714 – 720.
[26] *Biomineralisation and Biological Metal Accumulation* (Eds.: P. Westbroek, E. W. de Jong), Reidel, Dordrecht, **1983**.
[27] M. D. Ross, K. G. Pote, *Philos. Trans. R. Soc. London Ser. B* **1984**, *304*, 445 – 452.
[28] U. Lins, M. Farina, M. Kurc, G. Riordan, R. Thalmann, I. Thalmann, B. Kachar, *J. Struct. Biol.* **2000**, *131*, 67 – 78.
[29] C. G. Wright, D. G. Hubbard, *Acta Oto-Laryngol.* **1978**, *86*, 185 – 194.
[30] L. A. Everett, I. A. Belyantseva, K. Noben-Trauth, R. Cantos, A. Chen, S. I. Thakkar, S. L. Hoogstraten-Miller, B. Kachar, D. K. Wu, E. D. Green, *Hum. Mol. Genet.* **2001**, *10*, 153 – 161.
[31] P. Simon, D. Zahn, H. Lichte, R. Kniep, *Angew. Chem.* **2006**, *118*, 1945 – 1949; *Angew. Chem. Int. Ed.* **2006**, *45*, 1911 – 1915.
[32] P. Simon, W. Carrillo-Cabrera, P. Formanek, C. Göbel, D. Geiger, R. Ramlau, H. Tlatlik, J. Buder, R. Kniep, *J. Mater. Chem.* **2004**, *14*, 2218 – 2224.
[33] P. Simon, U. Schwarz, R. Kniep, *J. Mater. Chem.* **2005**, *15*, 4992 – 4996.
[34] H. Tlatlik, P. Simon, A. Kawska, D. Zahn, R. Kniep, *Angew. Chem.* **2006**, *118*, 1939 – 1944; *Angew. Chem. Int. Ed.* **2006**, *45*, 1905 – 1910.
[35] R. Kniep, P. Simon, *Angew. Chem.* **2008**, *120*, 1427 – 1431; *Angew. Chem. Int. Ed.* **2008**, *47*, 1405 – 1409.
[36] H. Cölfen, M. Antonietti, *Angew. Chem.* **2005**, *117*, 5714 – 5730; *Angew. Chem. Int. Ed.* **2005**, *44*, 5576 – 5591.
[37] *Biomineralisation: Cell Biology and Mineral Deposition* (Eds.: K. Simkiss, K. M. Wilbur), Academic Press, San Diego, **1989**.
[38] M. D. Ross, L.-G. Johnsson, D. Peacor, L. F. Allard, *Ann. Otol. Rhinol. Laryngol.* **1976**, *85*, 310 – 326.
[39] S. Mann, S. B. Parker, M. D. Ross, A. J. Skarnulis, R. J. P. Williams, *Philos. Trans. R. Soc. London Ser. B* **1983**, *218*, 415 – 424.
[40] D. Carlström, H. Engstrom, *Acta Oto-Laryngol.* **1955**, *45*, 14 – 18.
[41] D. Carlström, *Biol. Bull. Mar. Biol. Lab. Woods Hole MA US* **1963**, *125*, 441 – 463.
[42] C. P. Hommerich, R. Kniep: *Neue morphologische Befunde zum Wachstum der Otolithen*, 57. Jahresversammlung der Deutschen Gesellschaft für Hals-Nasen-Ohren-Heilkunde, Würzburg, 11 – 15. Mai, **1986**.
[43] C. D. Fermin, *Microsc. Res. Tech.* **1993**, *25*, 297 – 303.
[44] Instead of pure gelatine a mixture of agar and gelatine (weight ratio 7:3) was used as the gel matrix. The carbonate concentration in the L-shaped tube (see Experimental Section) was 0.133 mol L^{-1} Na_2CO_3 (no fluoride). All the other experimental conditions remained unchanged.

